PAPER

Experimental observation of kinetic Alfvén wave generated by magnetic reconnection

To cite this article: Peiyun Shi *et al* 2019 *Plasma Phys. Control. Fusion* **61** 125010

View the article online for updates and enhancements.

IOP ebooks™

Bringing you innovative digital publishing with leading voices to create your essential collection of books in STEM research.

Start exploring the collection - download the first chapter of every title for free.

Experimental observation of kinetic Alfvén wave generated by magnetic reconnection

Peiyun Shi[1] , **Kai Huang**[2]**, Quanming Lu**[2] **and Xuan Sun**[1]

[1] Department of Engineering and Applied Physics, University of Science and Technology of China, Hefei, 230026, People's Republic of China
[2] Department of Geophysics and Planetary Science, University of Science and Technology of China, Hefei 230026, People's Republic of China

E-mail: xsun@ustc.edu.cn

Abstract

The transient nature of magnetic reconnection dictates that it must be accompanied by rich electromagnetic wave activity, which can in turn affect the reconnection process. Interaction between Alfvén waves and reconnection has been simulated and recently observed in space. In this paper we report the first laboratory observation of a kinetic Alfvén wave (KAW) mode during reconnection in a linear device. The reconnection was measured by magnetic probes and the enhancement of light emission during reconnection was captured by a fast camera. The perpendicular wave pattern suggests it is an $m = -2$ mode rotating in ion diamagnetism direction. The wave data agrees with the theoretical prediction of KAW. The temporal correlation between KAW amplitude and reconnection rate indicates waves are generated by reconnection.

Keywords: magnetic reconnection, magnetic flux rope, kinetic Alfvén wave, electromagnetic waves

(Some figures may appear in colour only in the online journal)

1. Introduction

Magnetic reconnection, a process that can convert magnetic energy into thermal and kinetic energy, is responsible for many spectacular phenomena in nature [1, 2] as well as in the laboratories [3, 4]. Many studies have been conducted to understand the physics of reconnection but mostly in two dimensions. However, the successes accumulated from these studies have made it possible to tackle the more complex three dimensional processes. As Fujimoto *et al* [5] pointed out, adding a third dimension may open a new paradigm for studying reconnection. For example, the third dimension can allow waves to grow, which may facilitate reconnection or even play a dominant role in the presence of a guide field by opening up the outflow region [6]. Owing to its quadratic dispersive property, KAW radiated from the diffusion region is one of the candidates that can sustain such configuration for fast reconnection. Emission of Alfvén waves was also considered by Bellan [7] as a similar process to an antenna radiation, which is inherently 3D. It will inevitably generate

the radiation resistivity of diffusion region and lead to a faster reconnection rate.

Despite its important role in fast reconnection, KAW can contribute to wave-particles interactions in space because of its quasi-electrostatic feature. Particles can also be accelerated by its parallel electric field in the aurora, solar flare, etc [8]. Alfvén wave can be naturally generated by a reconnection [9]. Chaston *et al* [10, 11] discovered KAWs and drift Alfvén waves in magnetopause by using the Cluster spacecraft. They reported that KAWs radiated from the diffusion region and then changed to the perpendicular direction in the reconnection plane [10]. Using the recently launched MMS (Magnetospheric Multiscale Mission) spacecraft, Gershman *et al* [12] also found KAWs in the reconnection exhaust region and confirmed the presence of wave-particle energy exchange.

The importance of the Alfvén wave has also been recognized in recent computer simulations [13, 14]. KAW only exists in three dimensions and so has evaded most two dimensional simulations. Using 3D code, Liang *et al* [13] identified the existence of KAW in a finite guide field, which
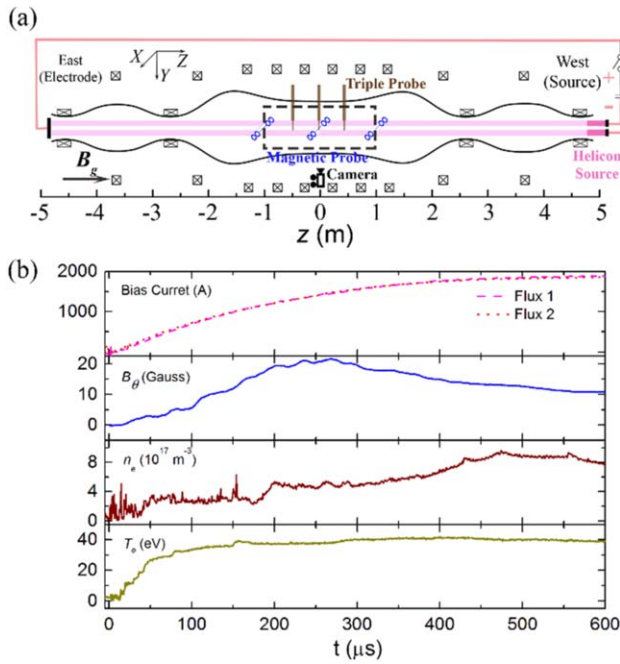
Figure 1. (a) Schematic showing the experiment of flux ropes (two pink columns) reconnecting in the KMAX device. The dashed box indicates the experimental region, and the black lines are the magnetic flux profile. Also shown are the positions of the triple probes (brown), magnetic probe array (blue), and fast camera. (b) Time histories of plasma parameters during reconnection: bias currents, reconnection magnetic field, electron density, and electron temperature.

radiated from a reconnection site with a perpendicular wavelength much smaller than the parallel wavelength. These results are similar to the results that we will report later in this paper.

Past laboratory experiments have studied the effects of whistler and hybrid waves [15–18], and there are limited reports of KAW observations in laboratory [19], whereas in this paper we report for the first time the detailed observation of KAW mode generated by laboratory reconnection in a linear device. The experimental setup and the evolution of the magnetic flux as well as the visible light intensity during magnetic reconnection are presented in section 2. In section 3 we show the $m = -2$ structure of the waves with frequency near the ion cyclotron frequency and its propagation, and then the comparison between our experiments and theories on KAW. In addition, temporal correlation between magnetic reconnection rate and the KAW's amplitude is provided to demonstrate that KAW is generated by magnetic reconnection process. Finally, we summarize in section 4.

2. Experimental setup for magnetic reconnection

The reconnection was realized by creating two mutually attracting flux ropes in a linear mirror device, KMAX [20], as shown in figure 1(a). The experimental region for this experiment was $z = [-1, 1]$ m, where the magnetic field was almost uniform. More details of such reconnection studies can

be found in Kulsrud's book [21], or in the RSX [22] and the LAPD [23] experiments. In our experiment, the two plasma columns were produced by two helicon plasma sources at the west end. Typical time evolutions of the currents are plotted in figure 1(b) for a bias voltage of 650 Volt, or a current of 1700 Ampere. Note the two current traces are almost identical, so they overlap in this plot.

Figure 1(b) shows the time traces of plasma density and electron temperature measured by a triple probe at $z = 0$ and $r = 0$ cm. At $t = 100$ μs, $n_e \sim 3 \times 10^{17}$ m^{-3} and $T_e \sim 30$ eV, about ten times the value before applying bias. The working gas was argon with pressure of 0.02 Pascal, and the background field in the central cell was 380 Gauss, i.e. ion gyro frequency $f_{ci} \sim 14$ kHz. Assuming $T_i \sim 0.2$ eV, the ion neutral collision time $\tau_{in} \sim 260$ μs, was larger than ion gyration time $\tau_{ci} \sim 70$ μs. From these measurements, some important parameters can be estimated: the ion Larmor radius $\rho_{cs} \sim 13$ cm using the ion sound speed $C_S \sim 11$ km s^{-1}, the Alfvén speed $V_A^{recx} \sim 4 - 7$ km s^{-1} for the reconnecting magnetic field $B^{recx} \sim 5 - 10$ Gauss, the diffusion time $\tau_\eta \sim 1$ ms, the Alfvén time $\tau_A \sim 8 - 13$ μs, where the plasma size $L \sim 10$ cm; the Lundquist number $S = \tau_\eta/\tau_A \sim 80 - 125$, and the effective plasma size $\lambda = L/\rho_{cs} \sim 0.8$. These values render our experiment fall into the regime of single X-line collisionless reconnection in the phase diagram proposed by Ji *et al* [24]. Meantime, it is worth noting that $\lambda < 1$ might complicate the rigorous analysis of magnetic reconnection.

Reconnection can produce a burst of light intensity, which in turn can be used to identify the reconnection region [25]. Figure 2(a) shows the burst of light intensity during reconnection in our experiment. The visible light image was recorded by a fast camera with sampling rate of 320 kHz. The flux ropes begin to approach each other at $t = 25$ μs and then merge into a single flux rope at $t = 100$ μs. The brightest spot indicates the formation of a current filament, which continues to illuminate until $t \sim 200$ μs. After that, the light intensity starts to decrease despite that the axial current continues to rise. Hence, the evolution of the light intensity is clearly related to the energy releasing during reconnection process. Similar phenomena were also observed in other laboratories [26, 27], and this result confirmed that the change of light intensity is associated with change in magnetic topology, as shown in figure 2(b).

The topology change of magnetic field was measured with a radially movable magnetic probe containing 14 coils in x direction and 14 coils in y direction. The spatial resolution was 1.5 cm. The probe was scanned in y-direction to obtain the 2D structure of magnetic fields. As shown in figure 2(b), the measured magnetic fields (shown by cyan arrows) are traced by magenta streamlines, and the color represents induced electric field, $E \sim -0.8$ V m^{-1} in the diffusion region, equivalent to ~ 0.1 in terms of the normalized reconnection rate, $E/(V_A^{recx}B^{recx})$. The rate is comparable to the values obtained in other experiments [28]. Note that the electric field measurements are derived from the vector potential, inferred from the measured magnetic field. The total annihilated private flux between $z = -1$ and 1 m is roughly
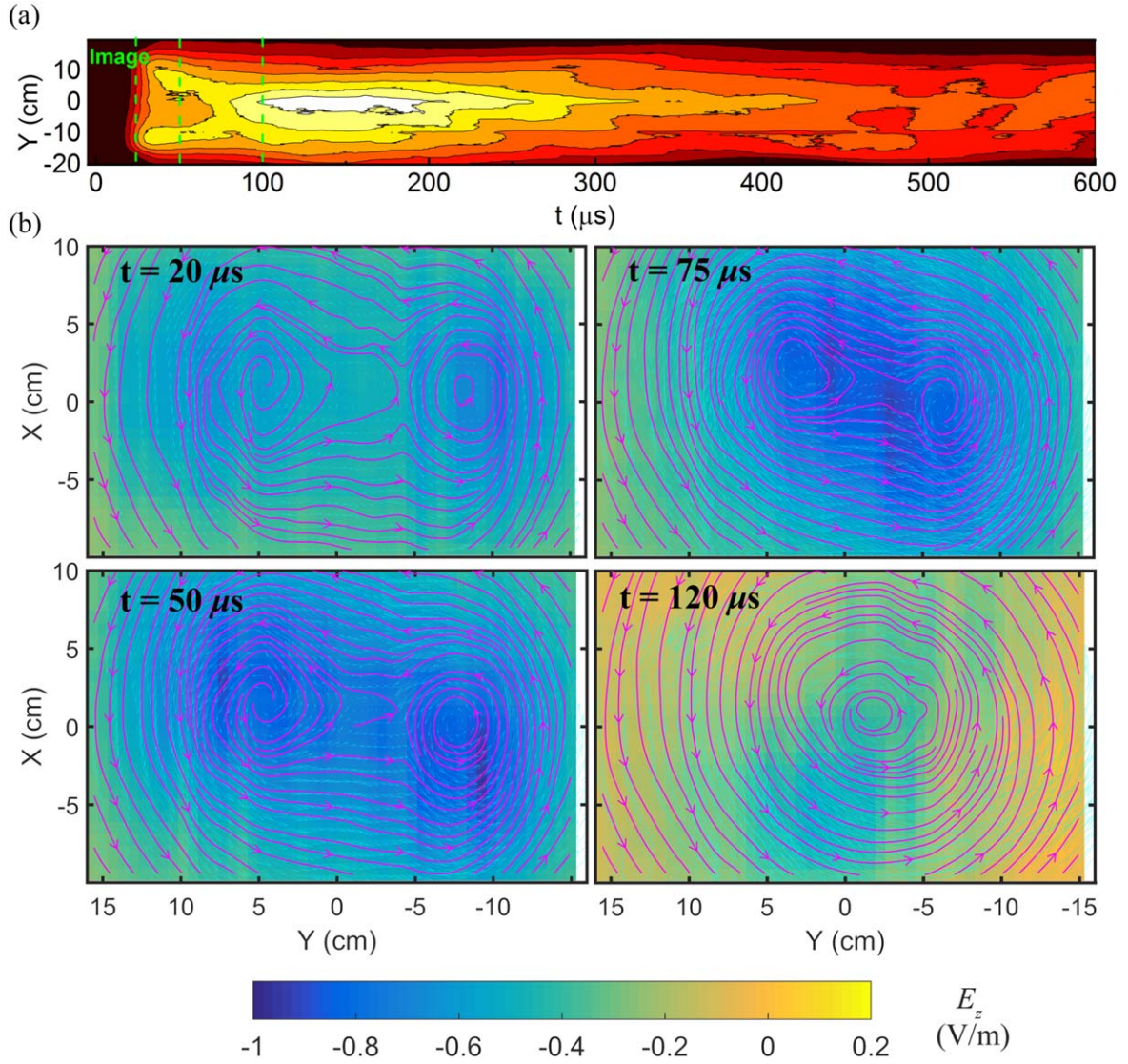
Figure 2. (a) Visible-light image recorded by a fast camera at $z = 0$ m. The time evolution of brightness is related to the energy release of reconnection. (b) Time evolution of flux rope merging. Magenta lines are traced from the measured B_x and B_y data in cyan. The measurement plane contains 616 data points. The color represents the strength of the calculated induced electric field.

0.1–0.2 mWb in 100 μs, or 8–30 mJ in 100 μs, equivalent to 0.05–0.2 MW m^{-3}.

Most of the released magnetic energy could be transferred to the particles, resulting in increasing of light emission, as evidenced in figure 2(a). It can also excite a variety of waves [5], offering a rich research area. In this paper we investigate waves with frequency near the ion cyclotron frequency and with perpendicular wavelength comparable to ρ_{cs}.

3. Wave generated by magnetic reconnection

In fact, the transient nature of reconnection process dictates that there must be accompanying wave activities. Though guide field can impede the reconnection, dispersive waves such as whistler or KAW can facilitate this process by opening up the exhauster region. According to Rogers *et al* [6], two critical parameters that determine the dependence of

the dispersive wave on the guide field are:

$$\mu_k = \frac{V_A^2 + C_S^2}{V_{AK}^2} \frac{m_e}{m_i}; \ \beta_k / 2 = \frac{C_S^2}{V_{AK}^2},$$

where $V_{AK} = \frac{\mathbf{B} \cdot \mathbf{k} / k}{\sqrt{\mu_0 \rho}} \approx V_A^{recx}$. In our circumstance, $\mu_k \sim 0.02 \ll 1$, $\beta_k / 2 \sim 3$, so both KAW and whistler wave can exist.

3.1. Wave's $m = -2$ structure

To restrict our study on low frequency waves, close to f_{ci}, we applied a bandpass filter [8, 15 kHz] to the magnetic data. Figure 3 shows the magnetic components of such a wave at $z = 0$ m and $t = 70$ μs as magenta streamlines, with raw data in cyan, and the color represents the wave currents derived from curl of wave magnetic field. Note that the amplitude of filtered wave is about 10% of reconnecting magnetic field. The two yellow regions correspond to the forward currents, while the reversed currents are located in the upper-right and lower-left
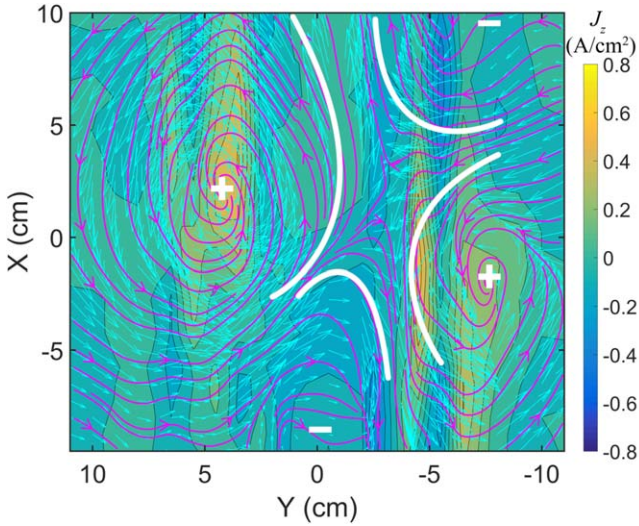
Figure 3. Measured KAW pattern at $z = 0$ m and $t = 70$ μs. Magenta streamlines are traced from the measured magnetic field vector (in cyan). The cusp configuration, with bold white lines drawn to facilitate viewing, indicates that it is an $m = -2$ mode. The background color represents the wave current j_z, and the plus sign is defined by the direction along the $+z$ axis.
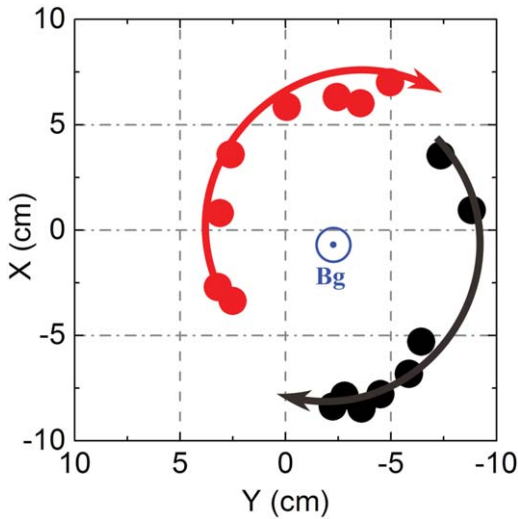
Figure 4. Rotation of the KAW (in the ion diamagnetic direction) is depicted by tracking this pattern over time. The red (black) solid circles are the approximate midpoints between the upper (lower) + and—currents. The main purpose of this plot is to show rotation of the pattern.

regions, just outside of our measurable area. The cusp-like configuration is highlighted by bold white lines, clearly revealing the $m = -2$ mode in a cylindrical geometry [29]. The negative sign is identified by tracking the rotation direction of this pattern over time, as shown in figure 4. In other words, the wave rotates in the ion diamagnetic direction with azimuthal wavenumber $k_\theta \sim -25$ rad m^{-1} at $r = 8$ cm. With the perpendicular wavelength comparable to the ion sound gyro radius, charge separation can occur because of orbit effect of ions, and a parallel electric field can be developed to neutralize the charges. Consequently, the ideal MHD wave mode, such as the Alfvén mode, will be coupled with longitude electrostatic

mode, and become the kinetic mode. The plasma parameter $\beta_e \sim 2.5 \times 10^{-3} > m_e/m_i \sim 1.4 \times 10^{-5}$ in this experiment also supports the existence of kinetic mode [30].

3.2. Wave's propagation feature and dispersion relation

The spatiotemporal evolution of this wave mode is shown in figure 5 for $z = -1, 0, 1$ m at four different times. Each plane contains 616 data points, with a spatial resolution of 1.5 cm × 1.0 cm, and the scanned area is 20 cm × 21 cm. Clearly the wave mode rotates in the ion cyclotron sense with $m = -2$, and there is a coherently phase delay along z, indicating that the wave propagates towards $+z$ direction. The parallel wavenumber $k_\|$ is inferred from the phase difference of the wave pattern in the z direction. The angles between the axis of the cusp structure and the x-axis at $z = -1, 0, 1$ m for $t = 70$ μs, are plotted in the inset panel of figure 6, and its slope yields $k_\| \sim 0.2$ rad m^{-1}. The data are then compared with Alfvén dispersion relation containing the Hall and the finite temperature effect [30]

$$
\begin{aligned}
&[\omega^2(1 + k^2\delta_e^2) - V_A^2 k_\|^2] \cdot [\omega^2(1 + k^2\delta_e^2)(\omega^2 - C_S^2 k^2) \\
&\quad - V_A^2 k^2(\omega^2 - C_S^2 k_\|^2)] \\
&= \left(\frac{\omega}{\Omega_{ci}}\right)^2 V_A^4 k^2 k_\|^2 (\omega^2 - C_S^2 k^2),
\end{aligned}
$$

where δ_e is the electron inertial length, $k = \sqrt{k_\|^2 + k_\perp^2}$, V_A is the Alfvén speed using the total magnetic field including B_g and B^{recx}. The kinetic effect becomes important when $k_\perp \rho_{cs} \gtrsim 1$. By including the finite temperature effect, the Alfvén wave can exceed the ion cyclotron frequency [29]. The dispersion relation is plotted in figure 6 with dimensionless axes ω/Ω_{ci} and $\omega/V_A k_\|$. In this figure, the dashed black lines are the upper and the lower boundaries of $\omega/V_A k_\|$ derived from the data: $T_e = 32 \pm 3$ eV, $n_e \sim (3 \pm 1) \times 10^{17}$ m^{-3}, and $k_\perp = 25 \pm 4$ rad m^{-1}, while the black square is the measured result, which falls within the predicted range. The neutral density effect [31] in our experiment is also included by modifying the Alfvén velocity $V_A^{eff} = V_A/\sqrt{A}$, with the mass loading factor $A = 3$. To further verify the dispersion relation, we changed guide fields to 270, 180 Gauss, and their corresponding predictions and measured results are also given in figure 6 in the same manner as red and blue colors respectively, which are also in good agreement with the model.

Finally, we shall show that the mode structure, azimuthal number $m = -2$ and location of magnetic vortices, are consistent with radial boundary condition in laboratory plasma. In free space or if the perpendicular wavelength is much smaller than plasma radius, the mode can propagate freely. However, in our case, a standing wave structure is developed in the radial direction because of the boundary effect. We apply the plasma-vacuum boundary condition, $J_r^{plasma} = J_r^{vacuum} = 0$, to the wave solution in the cylindrical geometry [29]:

$$
J_r = \frac{i}{\mu_0}\left(\left(1 + \frac{k_\|^2}{k_\perp^2}\right)\frac{mB_z}{r} + \frac{k_\|^2 G}{k_\perp^2 F}\frac{\partial B_z}{\partial r}\right),
$$

where $B_z = B_0 J_m(k_\perp r)$, J_m is m-order Bessel function of the first kind, $F = A - k_\|^2$, $G = A\omega/\Omega_{ci}$, $A = \omega^2/V_A^2(1 - \omega^2/\Omega_{ci}^2)$.
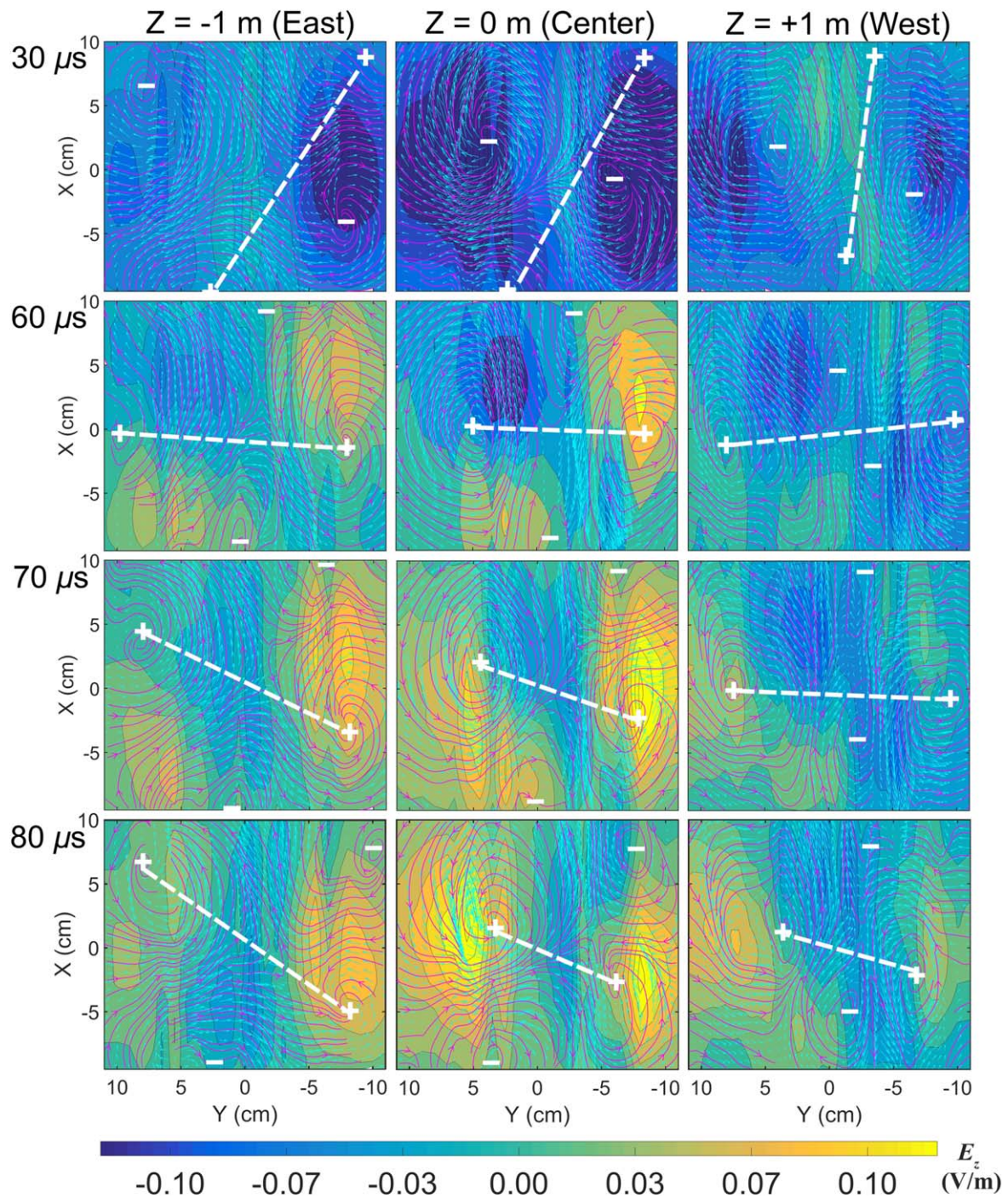
Figure 5. The spatiotemporal evolution of the $m = -2$ mode pattern. Dashed white lines, connecting two opposite 'o' points, are used to show the mode rotation (view along vertical direction) in the perpendicular plane and propagation along the $+z$ direction (view along horizontal direction). The color represents the wave electric field E_z.

By substituting plasma radius of 20 cm derived from the fast camera picture, one can find the first radial mode $k_\perp \sim$ 26 rad m^{-1}, and the location of magnetic vortices at $r = 10$ cm, which are both consistent with our measurement, *see* figures 3 and 5.

3.3. Temporal correlation between reconnection and wave

It is found in the experiment that the KAW appears only when magnetic reconnection occurs. To show the causal

relation between magnetic reconnection and KAW more quantitatively, we compare the amplitude of KAW and magnetic reconnection rate. The magnetic reconnection rate is described by calculating the decreasing rate of private magnetic flux owned by each individual flux rope [21]. Shown in figure 7 is the time evolution of the reconnection rate and KAW amplitude. Clearly the wave KAW is associated with magnetic reconnection and is generated by magnetic reconnection. In addition, the reconnection ratio can also be estimated by the ratio of inflow speed to Alfvén
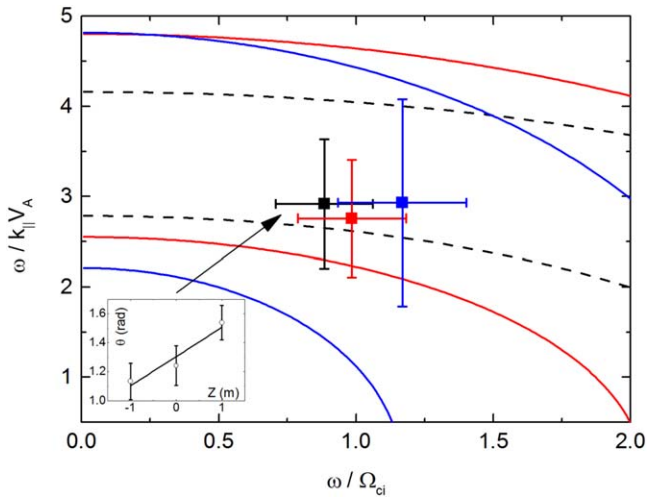
Figure 6. Comparison between the KAW dispersion relation (lines) and measurement (squares) under $B_g = 380$ (black), 270 (red), and 180 (blue) Gauss. Two lines of every color are for upper and lower estimations on dispersion relation. The inset shows an example of how $k_\parallel$ is extracted from the angle between the dashed lines in figure 5 and the x-axis at different z positions when $B_g = 380$ Gauss.
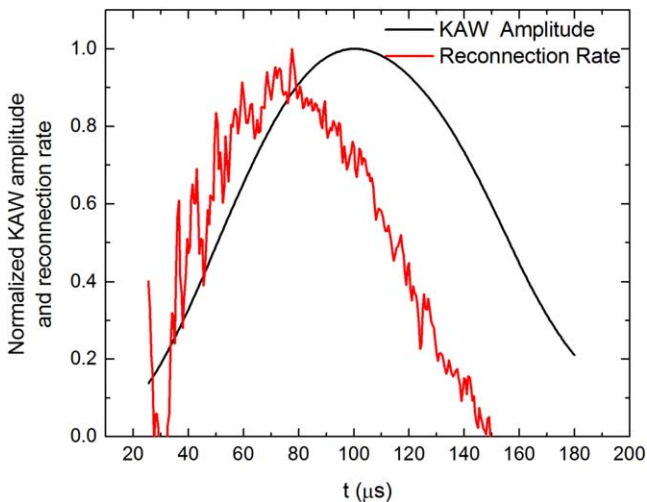
Figure 7. Temporal correlation between KAW amplitude and reconnection rate.

speed using reconnecting field component, which is 0.07–0.25 in this experiment.

4. Conclusion

In summary, we have for the first time observed the KAW during reconnection of laboratory plasma in a linear device. The reconnection process was measured by magnetic probes, corroborated by the light emission captured by a fast camera. The wave mode is confirmed by comparing measured wavenumbers with the prediction of KAW model. The time correlation between reconnection and wave amplitude suggests the KAW is generated by reconnection. Theoretic works have shown that KAW can enhance the reconnection rate in the presence of a guide field, while in our experiment both the

wave amplitude and reconnection rate grow over time and they may interact. This wave presents the pattern of the $m = -2$ mode, suggesting that it may be related to the bi-directional outflows from reconnection. Different from free space propagation, the boundary constrains the wave in the radial direction to a standing wave structure. The quadruple magnetic structure reminds us the Hall reconnection, which is hypothesized to be a KAW mode [14], however, this work demonstrate that KAW is not a reconnection in this case.

ORCID iDs

Peiyun Shi https://orcid.org/0000-0002-7129-278X
Xuan Sun https://orcid.org/0000-0002-8338-3654

References

[1] Priest E and Forbes T 2000 *Magnetic Reconnection: MHD Theory and Applications* (Cambridge: Cambridge University Press)
[2] Masuda S, Kosugi T, Hara H, Tsuneta S and Ogawara Y 1994 *Nature* **371** 495
[3] Yamada M, Kulsrud R and Ji H 2010 *Rev. Mod. Phys.* **82** 603
[4] Ding W X, Brower D L, Craig D, Deng B H, Fiksel G, Mirnov V, Prager S C, Sarff J S and Svidzinski V 2004 *Phys. Rev. Lett.* **93** 045002
[5] Fujimoto M, Shinohara I and Kojima H 2011 *Space Sci. Rev.* **160** 123
[6] Rogers B N, Denton R E, Drake J F and Shay M A 2001 *Phys. Rev. Lett.* **87** 195004
[7] Bellan P M 1998 *Phys. Plasmas* **5** 3081
[8] Hollweg J V 1999 *J. Geophys. Res. Space Phys.* **104** 14811
[9] Keiling A 2009 *Space Sci. Rev.* **142** 73
[10] Chaston C C, Johnson J R, Wilber M, Acuna M, Goldstein M L and Reme H 2009 *Phys. Rev. Lett.* **102** 015001
[11] Chaston C C *et al* 2005 *Phys. Rev. Lett.* **95** 065002
[12] Gershman D J *et al* 2017 *Nat. Commun.* **8** 14719
[13] Liang J, Lin Y, Johnson J R, Wang X and Wang Z-X 2016 *J. Geophys. Res. Space Phys.* **121** 6526
[14] Dai L, Wang C, Zhang Y, Lavraud B, Burch J, Pollock C and Torbert R B 2016 *Geophys. Res. Lett.* **44** 634–40
[15] Ji H, Terry S, Yamada M, Kulsrud R, Kuritsyn A and Ren Y 2004 *Phys. Rev. Lett.* **92** 115001
[16] Singh N 2011 *Phys. Rev. Lett.* **107** 245003
[17] Stechow A v, Grulke O and Klinger T 2016 *Plasma Phys. Control. Fusion* **58** 014016
[18] Dorfman S, Ji H, Yamada M, Yoo J, Lawrence E, Myers C and Tharp T D 2013 *Geophys. Res. Lett.* **40** 233

[19] Inomoto M, Kuwahata A, Tanabe H and Ono Y 2013 *Phys. Plasmas* **20** 061209

[20] Zhang Q, Shi P, Liu M, Lin M and Sun X 2015 *Fusion Sci. Technol.* **68** 50

[21] Kulsrud R M 2005 *Plasma Physics for Astrophysics* (Princeton: Princeton University Press)

[22] Sun X, Intrator T P, Dorf L, Sears J, Furno I and Lapenta G 2010 *Phys. Rev. Lett.* **105** 255001

[23] Gekelman W, De Haas T, Daughton W, Van Compernolle B, Intrator T and Vincena S 2016 *Phys. Rev. Lett.* **116** 235101

[24] Ji H and Daughton W 2011 *Phys. Plasmas* **18** 111207

[25] Wang H 1998 *Astrophys. J.* **509** 461

[26] Raymond A 2016 *PhD Thesis* University of Michigan

[27] Hansen J F, Tripathi S K P and Bellan P M 2004 *Phys. Plasmas* **11** 3177

[28] Cassak P A, Liu Y H and Shay M A 2017 *J. Plasma Phys.* **83** 715830501

[29] Cross R 1988 *An Introduction to Alfvén Waves* (Bristol and Philadelphia: Adam Hilger)

[30] Cramer N F 2011 *The Physics of Alfvén Waves* (Weinheim, FRG: Wiley-VCH Verlag GmbH & Co. KGaA)

[31] Watts C and Hanna J 2004 *Phys. Plasmas* **11** 1358